Trapping Devices of Carnivorous Fungus *Arthrobotrys oligospora* Can Isolate Heat-Triggered Excess Irons

Jiao Zhou,[⊥] Qunfu Wu,[⊥] Li Wu, Junxian Yan, Qianyi Cheng, Donglou Wang, Xuemei Niu*

State Key Laboratory for Conservation and Utilization of Bio-Resources in Yunnan, School of Life Sciences, Key Laboratory for Microbial Resources of the Ministry of Education, Yunnan University, Kunming 650091, P. R. China.

[⊥]These authors contributed equally to this paper

*To whom correspondence should be addressed. Tel: 86-871-65032538; Fax: 86-871-65034838. E-mail: xmniu@ynu.edu.cn (Xuemei Niu).

Abstract

The discovery of eukaryotes exhibiting an iron overload phenotype holds significant implications for developing treatments and strategies for human iron overload diseases caused by genetic defects. Under low-nutrient conditions, *Arthrobotrys oligospora* and other nematode-trapping fungi (NTF) can differentiate their mycelia into specialized structures for capturing prey as their nutritional source. Recent work has indicated that siderophore deficiency exacerbates the discrepancies between trapping device development and fungal carnivorous activity in *A. oligospora*, which has long been thought to represent a degeneration of the fungal carnivorous capacity. Using transmission electron microscopy combined with energy-dispersive X-ray spectroscopy, and functional analyses, we identified siderophore-deficient mutants that develop numerous trapping devices but lack a significant number of iron-containing ferrichrome granules and exhibit peroxisome development in the mycelia. Importantly, the characteristic electron-dense bodies in trapping devices store more iron compared to vacuoles and mitochondria. Genomic analysis indicated that NTFs lack the pivotal CccA-mediated vacuolar iron detoxification pathway that is conserved in most fungi. A Bayesian relaxed molecular clock analysis suggested that the evolutions of NTFs coincided with global warming. We demonstrated that the trapping devices of *A. oligospora*, triggered by high temperatures, can act as a system to sequester excess iron, thereby preventing abnormal free iron contents in mycelia and helping the fungi adapt to hot environments. Our findings reveal a non-trophic environmental factor that triggers iron overload and a diagnostic phenotypic indicator of iron overload in eukaryotes. This suggests that NTFs could serve as a potential eukaryotic model for elucidating the mechanisms of dynamic regulation of iron homeostasis, which could aid in treating iron overload-induced diseases in humans.

Key words: Trapping devices, Nematode-trapping fungi, *Arthrobotrys oligospora*, Iron overload, Heat, High temperature, Iron-sequestration

Main

The ability to segregate superfluous ingredients in response to environmental changes is essential for survival and fitness in all organisms. Iron overload results in cellular toxicity due to iron-generated oxyradicals and lipid membrane peroxidation[1]. A crucial means of iron storage in eukaryotes is ferritin or siderophore-mediated iron sequestration[2-4]. Ferritins serve as the primary iron storage system in animals, plants, and most microbes[5-7]. In the fungal kingdom, vacuolar iron storage, rather than siderophore-mediated storage, is the major iron detoxification mechanism due to its capacity to store iron[8, 9]. In *Saccharomyces cerevisiae*, iron is imported into the vacuole by the transporter Ccc1 for storage, reuse, and detoxification as ferric polyphosphate[10]. Inactivation of the Ccc1 homolog, *CccA*, in the human pathogenic fungus *Aspergillus fumigatus* greatly reduces resistance to iron toxicity[11]. Ccc1- or CccA-mediated vacuolar iron detoxification is particularly important for pathogenic fungi, which must adapt to grow inside warm-blooded hosts[4, 12, 13]. Could there be an alternative form of iron storage for iron overload in the living world? Temperature is a paramount environmental and climatic selective force that shapes morphological changes and biological processes, maintaining vital physiological and cellular functions[14-18]. However, the relationship between iron overload, storage, and temperature remains largely unknown.

In Ascomycota, a heterogeneous group of carnivorous fungi known as nematode-trapping fungi (NTFs) have evolved the ability to sense environmental changes, such as the presence of nematodes, under nutrient deprivation[19, 20]. This ability triggers the development of sophisticated nematode-trapping devices, enabling them to exploit nematodes, other small animals, and protozoans as their nutrient sources. NTFs belong to the Orbiliomycetes in Ascomycota, forming a monophyletic group with diverse trapping devices, including adhesive columns (AC), adhesive knobs (AK), adhesive networks (AN), and constricting rings (CR)[21, 22]. NTFs are among the most effective agents for controlling nematode populations and have been extensively studied for their potential as biological control agents for pathogenic nematodes[23]. While the development and behavior of trapping devices have been well-studied, increasing evidence suggests that the degeneration of carnivorous ability characterizes the evolution of NTFs[21]. The chemical properties of these trapping devices, however, have yet to be elucidated.

Fungal mycelia exhibit decision-making abilities, altering their developmental patterns in response to environmental changes by adjusting metabolic and cellular processes[24]. Mycelia can be microscopic or develop into visible structures, such as brackets, mushrooms, puffballs, rhizomorphs (long strands of hyphae cemented together), sclerotia (hard, compact masses), stinkhorns, toadstools, and truffles. At a certain stage, mycelia produce spores, either directly or through specialized fruiting bodies[25]. The trapping devices of nematode-trapping fungi develop from vegetative mycelia. Recent work has shown that a lack of siderophores or iron supplements triggers the development of trapping devices from mycelia in the NTF model species *Arthrobotrys oligospora*, but this damages the fungus's carnivorous ability[26]. However, the resulting cellular changes in the trapping device-forming mycelia remain unknown.

As our starting point, we investigated the cellular changes that occur in *A. oligospora* mycelia in response to the lack of siderophores. Previous work demonstrated that a large mass of electron-dense bodies is a diagnostic indicator for trapping devices[27, 28], but the chemical properties of these bodies remained unknown. To identify these properties, we conducted energy-dispersive X-ray spectroscopy combined with transmission electron microscopy, revealing that mycelia lost a large number of iron-containing ferrichrome granules while electron-dense bodies in trapping devices stored much more iron than vacuoles and mitochondria. The failure of vacuoles in iron storage led us to discover that all NTFs lack five key iron-related orthologous genes, including the pivotal vacuolar iron transporter *CccA* gene, which is widely distributed and highly conserved in fungi. A Bayesian relaxed molecular clock, based on 275,133 four-fold degenerate sites from 1,136 single-copy orthologous genes and three fossil calibration points, suggested that both the acquisition of siderophore biosynthesis and the divergence of fungal carnivorism from saprophytism coincided with global warming. Functional analysis exhibited that temperature reduction strongly inhibited trapping device development, even under iron treatments. Taken together, our work shows that due to a deficiency in vacuole-mediated iron storage, NTFs develop trapping devices to sequester excess iron from mycelia to avoid iron overload at high temperatures. More broadly, the development of trapping devices in *A. oligospora* to isolate excess iron at high temperatures can be regarded as analogous to human thermoregulation behavior: storing winter clothes in the closet when summer arrives and removing layers of clothing when the temperature rises. NTFs serve as a potential eukaryotic model to evaluate and develop agents and strategies for treating iron overload-induced diseases in humans.

Results

Desferriferrichrome for normal ferrichrome granules formation in mycelia

Most fungi, including *A. oligospora*, biosynthesize siderophores such as the widely distributed and well-known metabolite desferriferrichrome for iron uptake and storage[26, 29]. Recent work has demonstrated that two genes in *A. oligospora*, *Ao414* and *Ao415*, which encode L-ornithine N(5)-oxygenase and non-ribosomal peptide synthetase respectively, are responsible for the biosynthesis of desferriferrichrome derived from L-ornithine and glycine[26]. Deficiency in *Ao414* or *Ao415* caused the fungus to lose desferriferrichrome and trigger the mass production of trapping devices in two mutants, Δ*Ao414* and Δ*Ao415*, compared to the wild type (WT)[26]. Moreover, Δ*Ao414*, lacking any desferriferrichrome precursors, develops significantly more trapping devices than Δ*Ao415*, which has the desferriferrichrome precursor that can also sequester iron[26]. To better characterize the cellular changes that differentiate mycelia into trapping devices, we compared the structures in the mycelial cells between WT and the two mutants, Δ*Ao414* and Δ*Ao415*. TEM analysis revealed that Δ*Ao414* lost most iron-containing ferrichrome granules in the mycelial cells compared to WT (Fig. 1a–h). Meanwhile, Δ*Ao415* harbored aggregated large

iron-containing granules distinct from WT (Fig. 1a–d, i–l). Notably, peroxisomes formed in some cells of both Δ*Ao414* and Δ*Ao415* mycelia but not in those of WT (Fig. 1a–l), suggesting that the lack of desferriferrichrome could also trigger peroxisome development in mycelia. Furthermore, we confirmed that treatment with desferriferrichrome could restore normal ferrichrome granule formation in all mycelia of the two mutants, Δ*Ao414* and Δ*Ao415*, as well as WT (Fig. 1m–r).

Desferriferrichrome-mediated ferrichrome granules effectively for iron storage in mycelia

Energy-dispersive X-ray spectroscopy (EDX) is a widely used technique for studying the elemental composition and distribution in nanomaterials[30]. In this study, the EDX detector was incorporated into a transmission electron microscope (TEM) system to identify and quantify iron levels in ferrichrome granules within the fungal mycelial cells of both WT and the mutant Δ*Ao414*. Additionally, other organelles in these cells, including peroxisomes, vacuoles, mitochondria, and cell walls, were evaluated and compared with the ferrichrome granules. To better characterize the ferrichrome granules induced by desferriferrichrome, both WT and Δ*Ao414* were treated with and without desferriferrichrome.

We observed a significant Fe signal in the X-ray spectra from ferrichrome granules and mitochondria in both WT and Δ*Ao414* treated with or without desferriferrichrome, indicating that ferrichrome granules participate in iron storage alongside mitochondria (Fig. 2a–l and Extended Data Fig. S2). Interestingly, the absence of an Fe signal was also observed in the EDX spectra from peroxisomes or vacuoles in Δ*Ao414* treated with desferriferrichrome, in stark contrast to a notable Fe signal from peroxisomes in Δ*Ao414* treated with only solvent (Fig. 2k, l and Extended Data Fig. S2–3, 2–4). This distinct difference suggests that *A. oligospora* preferentially utilizes desferriferrichrome over peroxisomes or vacuoles for iron storage. Comparison of the relative iron levels in ferrichrome granules and other organelles within the same mycelial cells of both WT and Δ*Ao414* revealed that desferriferrichrome-mediated ferrichrome granules contained more iron than mitochondria and peroxisomes (Fig. 2m, p and Extended Data Fig. S2). These results indicate that desferriferrichrome plays a crucial role in iron storage within the mycelia.

Electron dense bodies in trapping devices mainly for iron storage and isolation

Trapping devices are characterized by the accumulation of numerous electron-dense bodies, whose components and physiological functions remain largely unknown. We observed that in WT trapping devices induced by nematodes, a large number of electron-dense bodies tend to concentrate in one of the two separated cells, whereas this was not observed in the mutants Δ*Ao414* and Δ*Ao415* (Fig. 3a–f). This suggests that desferriferrichrome regulates the aggregation and isolation of the electron-dense bodies in trapping devices. Additionally, iron supplementation led to a uniform morphology and size of the electron-dense bodies across all three strains—WT and the two mutants Δ*Ao414* and Δ*Ao415* (Fig. 3g–l).

Importantly, a significant Fe signal was observed in the EDX spectra from the electron-dense bodies in the trapping devices of WT induced by nematodes (Fig. 3m–p). Notably, the iron levels in these electron-dense bodies were substantially

higher than those in mitochondria and vacuoles within the same cells (Fig. 3o and Extended Data Fig. S3). To better compare the iron levels in electron-dense bodies and desferriferrichrome-mediated ferrichrome granules, we aimed to analyze cells containing both target organelles in adequate quantities and proper distribution. However, desferriferrichrome-mediated ferrichrome granules were primarily distributed in WT mycelia. We eventually found that cells from trapping devices of WT under iron treatment met these criteria effectively. The desferriferrichrome-mediated ferrichrome granules exhibited significantly higher iron levels than the electron-dense bodies in the same cells (Fig. 4a–d and Extended Data Fig. S4). Moreover, the desferriferrichrome-mediated ferrichrome granules were much smaller than the electron-dense bodies (Fig. 4e). These results suggest that while electron-dense bodies serve as an alternative system for iron storage and isolation, they are less efficient than desferriferrichrome-mediated ferrichrome granules but more efficient than mitochondria and vacuoles.

To further evaluate the role of trapping devices in iron storage and isolation, we compared the iron levels in the mycelia and trapping devices of WT and the mutant Δ*Ao414*. Collecting sufficient trapping devices and mycelia from a single plate to meet measurement requirements proved challenging. Additionally, the collected trapping devices frequently contained a substantial number of mycelia. Despite this, the combined sample of trapping devices and mycelia from both strains exhibited significantly higher levels of ferrous, ferric, and total iron compared to samples containing only mycelia (Fig. 4f, g). Notably, the ferric iron levels in the combined sample were 1.3-fold higher than those in the mycelia-only sample. Furthermore, the combined sample showed a markedly reduced ratio of ferrous to ferric iron compared to the mycelia-only sample (Fig. 4f, g).

Absence of key iron-related genes in NTFs

To explore the genetic mechanisms underlying the differentiation of mycelia into trapping devices for iron storage, we analyzed the distribution and abundance of genes involved in iron sequestration and transport in NTFs. We found that all NTFs lacked five specific orthologous genes: noranthrone synthase, siderophore biosynthesis acetylase, ferric-chelate reductase, metalloreductase, and the vacuolar iron transporter CccA (Fig. 5b and Supplementary Table S2). CccA is highly conserved across the fungal kingdom and is essential for importing iron into the vacuole to prevent toxic iron overload in the cytosol[10, 11, 31]. The observed dysfunction of vacuoles in *A. oligospora*, which prevents proper iron storage and thus avoids iron overload—a function typically performed by CccA-mediated vacuole iron storage in most fungi—supports the conclusion that NTFs lack CccA-mediated vacuolar iron storage.

Further analysis of ferritin, a ubiquitous iron storage protein found in both prokaryotes and eukaryotes[32-34], revealed variability in its copy numbers among species depending on the type of trapping devices in NTFs. Specifically, one copy is present in species with adhesive networks (*Arthrobotrys oligospora* and *Arthrobotrys flagrans*), two copies in species with constricting rings (*Drechslerella brochopaga* and *Drechslerella dactyloides*), three copies in species with adhesive columns (*Dactylellina cionopaga*), and four copies in species with adhesive knobs (*Dactylellina haptotyla* and *Dactylellina entomopaga*) (Fig. 5b). Notably, the transcriptional level of ferritin in *A. oligospora* is very low (average TPM = 4.19) and

is unaffected by the inactivation of *Ao414* (Extended Data Fig. S7). This suggests that the size and number of ferritin genes involved in iron sequestration and transport may contribute to the observed differences among NTFs.

Moreover, NTFs lack the ability to harbor ferrosomes, a class of iron storage organelles encoded by the fezABC operon found in various bacteria and archaea, such as *Desulfovibrio magneticus*. This deficiency is due to the presence of only the homologous gene FezB[35, 36], which encodes a P1B-6-ATPase, in NTFs. It is reasonable to assume that NTFs within the Orbiliomycetes class have developed alternative strategies to manage potential iron overload in their mycelia.

The evolutions of NTF coinciding with global high temperatures

Given the primary roles of ferrichrome and trapping devices in iron storage and isolation in *A. oligospora*, we investigated whether the origin of the *Ao415* gene cluster and the evolution of nematode-trapping fungi (NTFs) might be related to iron exposure. To elucidate the evolutionary trajectory of the *Ao415* cluster within the fungal kingdom, we conducted a comprehensive survey of cluster analogues containing the *Ao414* and *Ao415* genes across 1,488 high-quality fungal genomes (1,177 Ascomycota; 289 Basidiomycota; 21 Mucoromycota; 1 Zoopagomycota). We found that 744 fungal genomes contained homologs of the *Ao415* cluster, all of which were from Ascomycetes (Fig. 5a and Supplementary Table S3). A time-calibrated phylogenetic tree is required to further understand this evolution. However, the evolutionary origin of carnivorous fungi remains debated, with conflicting estimates of divergence times for fungal carnivorism in Orbiliomycetes (Ascomycota). This uncertainty may be attributed to: 1) inaccuracies in fossil calibrations, as the earliest known fossil of carnivorous fungi, *Palaeoanellus dimorphus*, dates to the early Cretaceous, approximately 100 million years ago[37]; 2) the limited number of genes analyzed[21, 22]; and 3) high variations in evolutionary rates among fungal lineages[38]. These issues could potentially be addressed by employing more precise rate estimation methods that utilize an adequate number of genes and focus exclusively on four-fold degenerate sites, which are largely neutral and exhibit a remarkable clock-like behavior[39, 40].

To address this phylogenetic challenge, we selected 16 representative fungi (9 Orbiliomycetes, 3 Pezizomycetes, 2 Eurotiomycetes, 1 Saccharomycetes, and 1 Taphrinomycetes) that contain the *Ao415* gene cluster, along with 1 fungus from Cystobasidiomycetes, which lacks the *Ao415* gene cluster, as an outgroup. We identified 1,136 sets of 1:1 orthologous protein-coding genes across these 17 fungal species and reconstructed a well-supported genome-wide phylogeny based on 1,141,520 concatenated amino acid positions (Extended Data Fig. S5a). Robust phylogenomic trees based on various codon positions were also generated (Extended Data Fig. S5b,c). Although the topologies of these phylogenetic trees were consistent and well-supported, significant discordance was observed in the topologies of single-gene trees (Extended Data Fig. S6). Such incongruence is often caused by incomplete lineage sorting (ILS), a common issue in the phylogenies of many animal groups that complicates phylogenetic inference[41]. To ensure the robustness of the reconstructed phylogeny despite ILS, we employed ASTRAL-III for a coalescent-based phylogenetic analysis using 1,136 orthologous gene trees. The topology of the resulting ASTRAL coalescent tree (Extended Data Fig. S5d) is identical to the genome-wide tree and aligns with the branching order of major groups

estimated in previous studies[22]. Our analysis further confirms that *Dactylella cylindrospora* is the closest extant relative of NTFs within Orbiliomycetes. This finding provides an excellent opportunity to identify the critical evolutionary forces associated with the origin of trapping devices during the early evolution of carnivorous fungi.

A time-calibrated phylogenetic tree, constructed using 275,133 four-fold degenerate sites from 1,136 single-copy orthologous genes, and calibrated with three major events[42]: Ascomycota crown group (487–773 Mya), Orbiliomycetes–other Pezizomycotina (353–554 Mya), Saccharomycotina crown group (276–514 Mya) and one fossil calibration point (node 9: >100 Mya)[37], indicated that the fungal lineage containing the *Ao415* cluster originated approximately 517 Mya (95% confidence interval (CI): 493.64−555.41 Mya). This timing aligns with a significant increase in ironstone during the early Ordovician (Fig. 5c). Furthermore, carnivorous fungi with trapping devices are estimated to have diverged from their saprophytic relatives (e.g., *Dactylella cylindrospora*) around 258 Mya (CI: 231−287 Mya). We did not find a correlation between the distribution patterns of iron (using the number of ironstones as a proxy) over geological time and the origin of trapping devices in NTFs. Both our time-calibrated tree and previous studies suggest that the origin of trapping devices in nematode-trapping fungi coincided with the Permian-Triassic mass extinction. There is considerable evidence indicating that abrupt climate changes, including both warming and cooling, have been linked to mass extinction events throughout Earth's history[43-45]. Specifically, a sharp increase in global temperatures is associated with the Permian-Triassic mass extinction.

During this period, sea surface temperatures reached approximately 40 °C, with land temperatures likely fluctuating to even higher values[45]. Mapping the changes in global average temperatures throughout the Phanerozoic[46] onto the evolutionary trajectory of carnivorous fungi reveals that the divergence of species with trapping devices coincided with lethally high temperatures during the early Triassic Greenhouse (Fig. 5c). Notably, before the emergence of this nematode-trapping fungi (NTF) group, the ancestor of Orbiliomycetes experienced the longest ice age, known as the Late Paleozoic Ice Age (from 360 to 255 Mya)[47, 48]. During this period, the five crucial genes (encoding noranthrone synthase, siderophore biosynthesis acetylase, ferric-chelate reductase, metalloreductase, and CccA) involved in iron storage and sequestration were lost (Extended Data Fig. S8). Additionally, the emergence of the *Ao415* gene cluster occurred during a period of high temperatures in the Cambrian (Fig. 5c). Therefore, we hypothesize that the development of nematode-trapping structures in NTFs was an adaptation to high-temperature environments after loss of five pivotal iron related gene during the longest-lived ice age.

Temperature-dependence of trapping devices and iron compositions in *A. oligospora* mycelia

To date, the role of temperature changes in the development of trapping devices remains poorly understood. While many studies have suggested that temperature influences the growth of fungal mycelia, we specifically evaluated the growth of *A. oligospora* on PDA at four different temperatures: 28 °C, 24 °C, 20 °C, and 16 °C. *A. oligospora* displayed similar colony growths at both 28 °C and 20 °C, with slightly less growth compared to the peak growth observed at 24 °C. This suggests that the

optimal growth temperature for *A. oligospora* is 24 °C, and variations of ±4 °C have a comparable effect on colony growth (Fig. 6a). Further comparisons of WT and mutant *ΔAo414* strains cultivated at 28 °C, 20 °C, and 12 °C demonstrated that both strains exhibited robust temperature-dependent mycelial growth (Fig. 6b). Additionally, we observed notable temperature-dependent development of trapping devices in both WT and *ΔAo414* strains at the same three temperatures (Fig. 6c).

Recent studies suggest that temperature variations can influence free iron content and trigger metabolic changes in thermophilic fungi[26, 49]. We hypothesized that iron might play a key role in the temperature-dependent development of trapping devices in *A. oligospora*. To investigate this, we compared the iron levels and iron ratios in the mycelia of both WT and mutant *ΔAo414* strains at three different temperatures: 28 °C, 20 °C, and 12 °C. We observed that the *ΔAo414* mutant spontaneously developed numerous trapping devices at 28 °C, which may account for the low ferric levels in *ΔAo414* mycelia at this temperature (Fig. 6c, d). The *ΔAo414* mutant exhibited significantly increased ferric levels at 20 °C and 12 °C compared with WT, consistent with its inability to synthesize desferriferrichrome for ferric sequestration (Fig. 6d). Consequently, the *ΔAo414* mutant had extremely low iron ratios of ferrous to ferric iron at 20 °C and 12 °C compared with WT. Notably, WT exhibited the highest levels of ferrous and total free iron, as well as the highest iron ratios of ferrous to ferric iron, at 12 °C, with the opposite trend observed at 28 °C (Fig. 6e). This indicates that the iron content in WT mycelia is negatively correlated with temperature.

Discussion

The ability to isolate and temporarily store unwanted components to adapt to environmental changes is a fundamental aspect of homeostasis regulation in all living organisms. Hemochromatosis is a disorder characterized by iron overload resulting from inherited or acquired factors[50, 51]. Without treatment, excess iron can damage various organs, including the liver, heart, pancreas, endocrine glands, and joints, potentially leading to cirrhosis, liver failure, cancer, arthritis, diabetes, and heart failure[50, 52]. Caucasians are more susceptible to developing iron overload and the associated complications of hemochromatosis due to a higher prevalence of mutations in the homeostatic iron regulator gene within this population, which leads to excessive iron absorption[53, 54]. Recently, research has increasingly focused on discovering new molecules and mechanisms for managing iron, controlling its availability, and mitigating its intrinsic toxicity as a means to improve treatment for iron overload.

In this study, we found that high temperatures are a significant factor in triggering excess iron in the NTF *A. oligospora*. Our results indicated that the WT mycelia of *A. oligospora* exhibited significantly lower levels of total iron and a decreased ratio of ferrous to ferric iron at high temperatures compared to low temperatures. This observation aligns with recent research demonstrating that relative cold stress significantly increases total iron levels and the ratio of ferrous to ferric iron in the mycelia of thermophilic fungi such as *Thermomyces* species[49]. This suggests a negative correlation between temperature and iron content in fungal mycelia. It is reasonable to conclude that *A. oligospora* has adapted to low temperatures by accumulating higher total iron content to support sufficient energy production. Conversely, in response to subsequent high temperatures, the fungus reduces iron

levels by developing trapping devices for excess iron sequestration, which serves as a key strategy for climate adaptation.

We observed that temperature reduction or desferriferrichrome supplementation significantly inhibits trapping device development in *A. oligospora*, while iron supplementation or a deficiency in desferriferrichrome biosynthesis triggers mass trapping device formation. Importantly, the electron-dense bodies in trapping devices are less efficient for iron storage and isolation compared to desferriferrichrome-mediated ferrichrome granules, but more efficient than mitochondria and vacuoles, thus serving as an alternative iron storage system. A previous study also reported that electron-dense bodies in the alga *Cyanidium caldarium* function in iron storage[55]. This suggests that the involvement of electron-dense bodies in iron sequestration is likely a general phenomenon rather than specific to a single fungal strain. The primary difference between *A. oligospora* and *Cyanidium caldarium* is that the fungus develops specialized mycelial structures—trapping devices—for housing these electron-dense bodies. The development of trapping devices is considered a diagnostic marker for the transition from saprophytic to predatory lifestyles in NTFs and plays a crucial role in their carnivorous activity.

Historically, nutrient signals have been viewed as the primary triggers for trapping device formation[56]. However, the role of temperature in trapping device development has been underexplored, despite its critical impact on fungal phenotype and diversity. This study demonstrates that temperature is a key non-nutrient environmental factor influencing trapping device formation through its regulation of iron homeostasis in *A. oligospora*. Recent work suggests that phylogenetic analysis of the protein Ao415 indicates that NTFs are most closely related to *Kalaharituber pfeilii* (a desert truffle), *Tricharina praecox* (cup fungus), *Trichophaea hybida* (cup fungus), *Morchella sextelata* (a true morel), *Morchella importuna* (a true morel), *Choiromyces venosus* (a truffle), and *Tuber borchii* (a truffle)[26]. Most of these fungi produce valuable and edible fruiting bodies. Our findings that the development of trapping devices in *A. oligospora* serves as a key climate mitigation strategy for sequestering excess iron to adapt to high temperatures may provide insights into the mechanisms underlying fruiting body formation in these valuable fungi.

In summary, we have identified temperature as a key non-nutrient environmental factor in triggering excess iron accumulation and trapping device development in *A. oligospora*. The trapping devices in *A. oligospora* represent unprecedented iron storage structures that sequester excess iron from the mycelia to mitigate the effects of high temperatures. Unlike known iron sequestration granules or organelles within cells, these trapping devices are distinct morphological structures that differentiate from the mycelia. The electron-dense bodies within the trapping devices function as the primary granules for iron sequestration. These iron-sequestering structures offer a novel prototype for microbial iron systems. Thus, NTFs present a valuable eukaryotic model for developing innovative agents and therapies for treating iron overload-associated diseases.

Funding
This work was sponsored by Program 202201BF070001-012 of “Double tops” from Yunnan Province and Yunnan University and 2022KF001 from State Key Laboratory

for Conservation and Utilization of Bio-Resources in Yunnan. This work was sponsored by National Natural Science Foundation of China 21977086 and 21867018, Yunnan University Program awarded to X.N. (XT412003).

Acknowledgments: We would like to thank the School of Chemical Science and Technology, Key Laboratory of Medicinal Chemistry for Natural Resource - Ministry of Education, Yunnan University for providing us with TEM-EDX. We wish to thank Longchun Bian, for support with the Energy Dispersive X-ray Spectroscopy analyses and data reduction. We would like to thank the Institutional Center for Shared Technologies and Facilities of Kunming Institute of Zoology, Chinese Academy of Sciences, for providing us with transmission electron microscopy. We are grateful to Yingqi Guo for her great help in preparing TEM samples and taking/analyzing TEM images.

Competing Interests: The authors declare no competing interests.

Associated content

Supporting Information available. Additional figures and tables as mentioned in the text.

Data availability

Our sequences files of transcriptome are accessible from the National Center for Biotechnology Information (NCBI) under BioProject accession: PRJNA639935 (https://www.ncbi.nlm.nih.gov/bioproject/PRJNA1073725).

References:

1. Galy, B., Conrad, M. & Muckenthaler, M. Mechanisms controlling cellular and systemic iron homeostasis. *Nat Rev Mol Cell Biol* **25**, 133-155 (2024).
2. Li, H. et al. Advancements of nature nanocage protein: preparation, identification and multiple applications of ferritins. *Crit Rev Food Sci Nutr* **62**, 7117-7128 (2022).
3. Lampe, R. H., Coale, T. H., McQuaid, J. B. & Allen, A. E. Molecular mechanisms for iron uptake and homeostasis in marine eukaryotic phytoplankton. *Annu Rev Microbiol* (2024).
4. Misslinger, M., Hortschansky, P., Brakhage, A. A. & Haas, H. Fungal iron homeostasis with a focus on *Aspergillus fumigatus*. *Biochim Biophys Acta* **1868**, 118885 (2021).
5. Arosio, P., Elia, L. & Poli, M. Ferritin, cellular iron storage and regulation. *IUBMB Life* **69**, 414-422 (2017).
6. Honarmand Ebrahimi, K., Bill, E., Hagedoorn, P. L. & Hagen, W. R. The catalytic center of ferritin regulates iron storage via Fe(II)-Fe(III) displacement. *Nat Chem Biol* **8**, 941-948 (2012).
7. Yi, W. et al. Ferritin-mediated mitochondrial iron homeostasis is essential for the survival of hematopoietic stem cells and leukemic stem cells. *Leukemia* **38**, 1003-1018 (2024).
8. Gerwien, F., Skrahina, V., Kasper, L., Hube, B. & Brunke, S. Metals in fungal virulence. *FEMS Microbiol Rev* **42**, fux050 (2018).
9. Sorribes-Dauden, R., Peris, D., Martínez-Pastor, M. T. & Puig, S. Structure and function of the vacuolar Ccc1/VIT1 family of iron transporters and its regulation in fungi. *Comput Struct Biotechnol J* **18**, 3712-3722 (2020).
10. Li, L., Chen, O. S., Ward, D. M. & Kaplan, J. CCC1 Is a transporter that mediates vacuolar iron storage in yeast. *J Biol Chem* **276**, 29515-29519 (2001).
11. Gsaller, F. et al. The interplay between vacuolar and siderophore-mediated iron storage in *Aspergillus fumigatus*. *Metallomics* **4**, 1262-1270 (2012).
12. Pijuan, J. et al. Regulatory and pathogenic mechanisms in response to iron deficiency and excess in fungi. *Microb Biotechnol* **16**, 2053-2071 (2023).
13. Blatzer, M. & Latgé, J. P. Metal-homeostasis in the pathobiology of the opportunistic human fungal pathogen *Aspergillus fumigatus*. *Curr Opin Microbiol* **40**, 152-159 (2017).
14. Sur, S., Sharma, A. Understanding the role of temperature in seasonal timing: Effects on behavioural, physiological and molecular phenotypes. *Mol Ecol* **00**, e17447 (2024).
15. Ma, C. S., Ma, G. & Pincebourde, S. Survive a warming climate: Insect responses to extreme high temperatures. *Annu Rev Entomol* **66**, 163-184 (2021).
16. Knapp, B. D. & Huang, K. C. The effects of temperature on cellular physiology. *Annu Rev Biophys* **51**, 499-526 (2022).
17. Dohnalová, H., Matoušková, E. & Lankaš, F. Temperature-dependent elasticity of DNA, RNA, and hybrid double helices. *Biophys J* **123**, 572-583 (2024).
18. Trip, D. S. L. & Youk, H. Yeasts collectively extend the limits of habitable temperatures by secreting glutathione. *Nat Microbiol* **5**, 943-954 (2020).
19. Yang, Y., Yang, E., An, Z. & Liu, X. Evolution of nematode-trapping cells of predatory fungi of the Orbiliaceae based on evidence from rRNA-encoding DNA and multiprotein sequences. *Proc Natl Acad Sci USA* **104**, 8379-8384 (2007).
20. Niu, X. M. & Zhang, K. Q. *Arthrobotrys oligospora*: a model organism for understanding the interaction between fungi and nematodes. *Mycology* **2**, 59-78 (2011).
21. Yang, E. et al. Origin and evolution of carnivorism in the Ascomycota (fungi). *Proc Natl Acad Sci*

USA **109**, 10960-10965 (2012).
22. Ji, X. et al. Expansion of adhesion genes drives pathogenic adaptation of nematode-trapping fungi. *iScience* **23**, 101057 (2020).
23. Pokhare, S. S., Mhatre, P. H., Manjunatha, N., Patil, D. & Agarrwal, R. in Sustainable Management of Nematodes in Agriculture, Vol.2: Role of Microbes-Assisted Strategies. (eds. K.K. Chaudhary, M.K. Meghvansi & S. Siddiqui) 183-206 (Springer International Publishing, Cham; 2024).
24. Naranjo-Ortiz, M. A. & Gabaldón, T. Fungal evolution: cellular, genomic and metabolic complexity. *Biol Rev* **95**, 1198-1232 (2020).
25. Porter, D. L. & Naleway, S. E. Hyphal systems and their effect on the mechanical properties of fungal sporocarps. *Acta Biomater* **145**, 272-282 (2022).
26. Zhou, J. et al. Rare NRPS gene cluster for desferriferrichrome biosynthesis controls the conflict between trap formation and nematicidal activity in *Arthrobotrys oligospora*. *J Agric Food Chem* **72**, 3560-3571 (2024).
27. Veenhuis, M., Nordbring-Hertz, B. & Harder, W. An electron-microscopical analysis of capture and initial stages of penetration of nematodes by *Arthrobotrys oligospora*. *Antonie Van Leeuwenhoek* **51**, 385-398 (1985).
28. Xie, M. et al. *Fus3* regulates asexual development and trap morphogenesis in the nematode-trapping fungus *Arthrobotrys oligospora*. *iScience* **26** (2023).
29. Hider, R.C. & Kong, X. Chemistry and biology of siderophores. *Nat Prod Rep* **27**, 637-657 (2010).
30. Hodoroaba, V. D. in Characterization of Nanoparticles. (eds. V.-D. Hodoroaba, W.E.S. Unger & A.G. Shard) 397-417 (Elsevier, 2020).
31. Lapinskas, P. J., Lin, S. J. & Culotta, V. C. The role of the *Saccharomyces cerevisiae* CCC1 gene in the homeostasis of manganese ions. *Mol Microbiol* **21**, 519-528 (1996).
32. Briat, J. F. & Lobréaux, S. Iron transport and storage in plants. *Trends Plant Sci* **2**, 187-193 (1997).
33. Briat, J. F., Duc, C., Ravet, K. & Gaymard, F. Ferritins and iron storage in plants. *Biochim Biophys Acta - Gen Subj* **1800**, 806-814 (2010).
34. Segond, D. et al. Iron acquisition in *Bacillus cereus*: The roles of IlsA and Bacillibactin in exogenous ferritin iron mobilization. *PLoS Path* **10**, e1003935 (2014).
35. Grant, C. R. et al. Distinct gene clusters drive formation of ferrosome organelles in bacteria. *Nature* **606**, 160-164 (2022).
36. Byrne, M. E. et al. *Desulfovibrio magneticus* RS-1 contains an iron- and phosphorus-rich organelle distinct from its bullet-shaped magnetosomes. *Proc Natl Acad Sci USA* **107**, 12263-12268 (2010).
37. Schmidt, A. R., Dörfelt, H. & Perrichot, V. *Palaeoanellus dimorphus* gen. et sp. nov. (Deuteromycotina): a Cretaceous predatory fungus. *Am J Bot* **95**, 1328-1334 (2008).
38. Shen, X. X. et al. Tempo and mode of genome evolution in the budding yeast subphylum. *Cell* **175**, 1533-1545.e1520 (2018).
39. Whitfield, J. B. Estimating the age of the polydnavirus/braconid wasp symbiosis. *Proc Natl Acad Sci USA* **99**, 7508-7513 (2002).
40. Langley, C. H. & Fitch, W. M. An examination of the constancy of the rate of molecular evolution. *J Mol Evol* **3**, 161-177 (1974).
41. Chen, L. et al. Large-scale ruminant genome sequencing provides insights into their evolution and distinct traits. *Science* **364**, eaav6202 (2019).
42. Beimforde, C. et al. Estimating the Phanerozoic history of the Ascomycota lineages: Combining fossil and molecular data. *Mol Phylogen Evol* **78**, 386-398 (2014).

43. Crowley, T. J. & North, G. R. Abrupt climate change and extinction events in Earth history. *Science* **240**, 996-1002 (1988).
44. Mayhew, P. J., Bell, M. A., Benton, T. G. & McGowan, A. J. Biodiversity tracks temperature over time. *Proc Natl Acad Sci USA* **109**, 15141-15145 (2012).
45. Sun, Y. et al. Lethally hot temperatures during the early Triassic greenhouse. *Science* **338**, 366-370 (2012).
46. Scotese, C. R., Song, H., Mills, B. J. W. & van der Meer, D. G. Phanerozoic paleotemperatures: The earth's changing climate during the last 540 million years. *Earth-Sci Rev* **215**, 103503 (2021).
47. Kent, D. V. & Muttoni, G. Pangea B and the Late Paleozoic Ice Age. *Palaeogeogr Palaeoclimatol Palaeoecol* **553**, 109753 (2020).
48. Montañez, I. P. & Poulsen, C. J. The Late Paleozoic Ice Age: An Evolving Paradigm. *Annu Rev Earth Planet Sci* **41**, 629-656 (2013).
49. Yang, X. et al. Melanin precursors mediated adaption to temperature changes in fungus and animal via inhibition of lipid-mediated ferroptosis. *Sci China Life Sci* **66**, 1800-1817 (2023).
50. Corradini, E., Buzzetti, E. & Pietrangelo, A. Genetic iron overload disorders. *Mol Aspects Med* **75**, 100896 (2020).
51. Camaschella, C. Understanding iron homeostasis through genetic analysis of hemochromatosis and related disorders. *Blood* **106**, 3710-3717 (2005).
52. Jomova, K. et al. Essential metals in health and disease. *Chem.-Biol Interact* **367**, 110173 (2022).
53. Adams Paul, C. et al. Hemochromatosis and iron-overload screening in a racially diverse population. *New Engl J Med* **352**, 1769-1778 (2005).
54. Motulsky, A. G. & Beutler, E. Population screening in hereditary hemochromatosis. *Annu Rev Public Health* **21**, 65-79 (2000).
55. Nagasaka, S., Nishizawa, N. K., Watanabe, T., Mori, S. & Yoshimura, E. Evidence that electron-dense bodies in *Cyanidium caldarium* have an iron-storage role. *BioMetals* **16**, 465-470 (2003).
56. Su, H. et al. Trapping devices of nematode-trapping fungi: formation, evolution, and genomic perspectives. *Biol Rev* **92**, 357-368 (2017).
57. He, Z. Q. et al. Polyketide synthase–terpenoid synthase hybrid pathway regulation of trap formation through ammonia metabolism controls soil colonization of predominant nematode-trapping fungus. *J Agric Food Chem* **69**, 4464-4479 (2021).
58. Sheraz, S. et al. Subcellular dynamics studies of iron reveal how tissue-specific distribution patterns are established in developing wheat grains. *New Phytol* **231**, 1644-1657 (2021).
59. Pertea, G. & Pertea, M. GFF utilities: GffRead and GffCompare [version 1; peer review: 3 approved]`. *F1000Research* **9** (2020).
60. Simão, F. A., Waterhouse, R. M., Ioannidis, P., Kriventseva, E. V. & Zdobnov, E. M. BUSCO: assessing genome assembly and annotation completeness with single-copy orthologs. *Bioinform* **31**, 3210-3212 (2015).
61. Blin, K. et al. antiSMASH 7.0: new and improved predictions for detection, regulation, chemical structures and visualisation. *Nucleic Acids Res* **51**, W46-W50 (2023).
62. Gilchrist, C. L. M. et al. cblaster: a remote search tool for rapid identification and visualization of homologous gene clusters. *Bioinform adv* **1**, vbab016 (2021).
63. Emms, D. M. & Kelly, S. OrthoFinder: phylogenetic orthology inference for comparative genomics. *Genome Biol* **20**, 238 (2019).

64. Edgar, R. C. Search and clustering orders of magnitude faster than BLAST. *Bioinform* **26**, 2460-2461 (2010).
65. Törönen, P., Medlar, A. & Holm, L. PANNZER2: a rapid functional annotation web server. *Nucleic Acids Res* **46**, W84-W88 (2018).
66. Minh, B. Q. et al. IQ-TREE 2: New models and efficient methods for phylogenetic inference in the genomic era. *Mol Biol Evol* **37**, 1530-1534 (2020).
67. Rambaut, A., Drummond, A. J., Xie, D., Baele, G. & Suchard, M. A. Posterior summarization in Bayesian phylogenetics using Tracer 1.7. *Syst Biol* **67**, 901-904 (2018).
68. Chen, S., Zhou, Y., Chen, Y. & Gu, J. fastp: an ultra-fast all-in-one FASTQ preprocessor. *Bioinform* **34**, i884-i890 (2018).
69. Kim, D., Paggi, J. M., Park, C., Bennett, C. & Salzberg, S. L. Graph-based genome alignment and genotyping with HISAT2 and HISAT-genotype. *Nat Biotechnol* **37**, 907-915 (2019).
70. Liao, Y., Smyth, G. K. & Shi, W. featureCounts: an efficient general purpose program for assigning sequence reads to genomic features. *Bioinform* **30**, 923-930 (2014).
71. Love, M. I., Huber, W. & Anders, S. Moderated estimation of fold change and dispersion for RNA-seq data with DESeq2. *Genome Biol* **15**, 550 (2014).

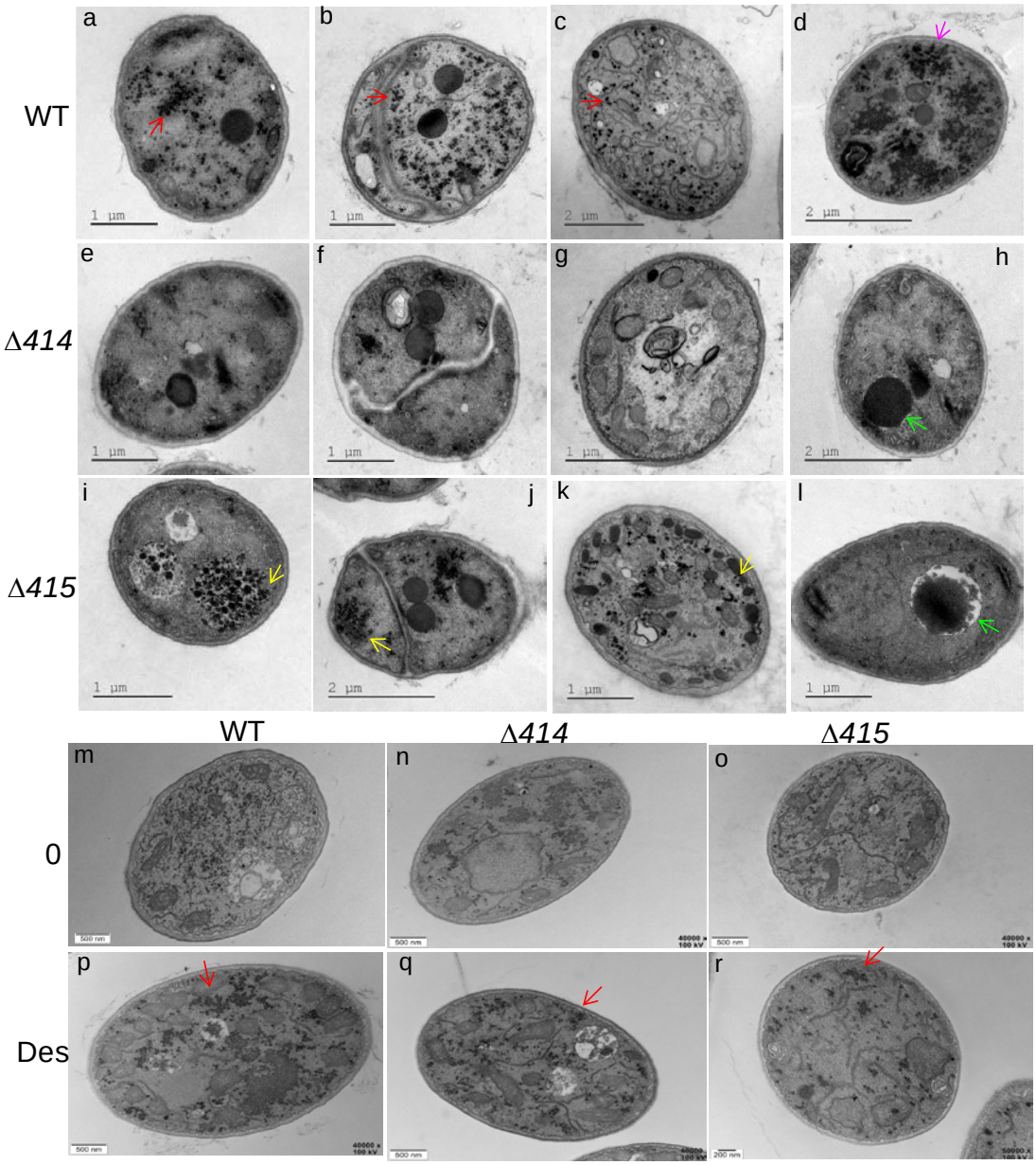

Fig. 1| TEM analysis of cellular changes in the fungal mycelia of *A. oligospora* in response to the loss and supplementation of desferriferrichrome. *ΔAo414* (*Δ414*) is deficient in the entire desferriferrichrome biosynthetic pathway, while *ΔAo415 (Δ415)* lacks only part of this pathway, specifically still producing desferriferrichrome precursors capable of iron chelation. **a–l**, Comparison of organelles in the mycelial cells of WT (**a–d**), Δ*Ao414* (**e–h**) and Δ*Ao415* (**i–l**). Red arrow: normal ferrichrome granules. Yellow arrow: abnormal ferrichrome granules. Green arrow: peroxisome. **m–r**, The effect of desferriferrichrome on organelles in mycelial cells of WT (**m, p**), Δ*Ao414* (**n, q**) and Δ*Ao415* (**o, r**). Des: desferriferrichrome solution. 0: solvent as control.

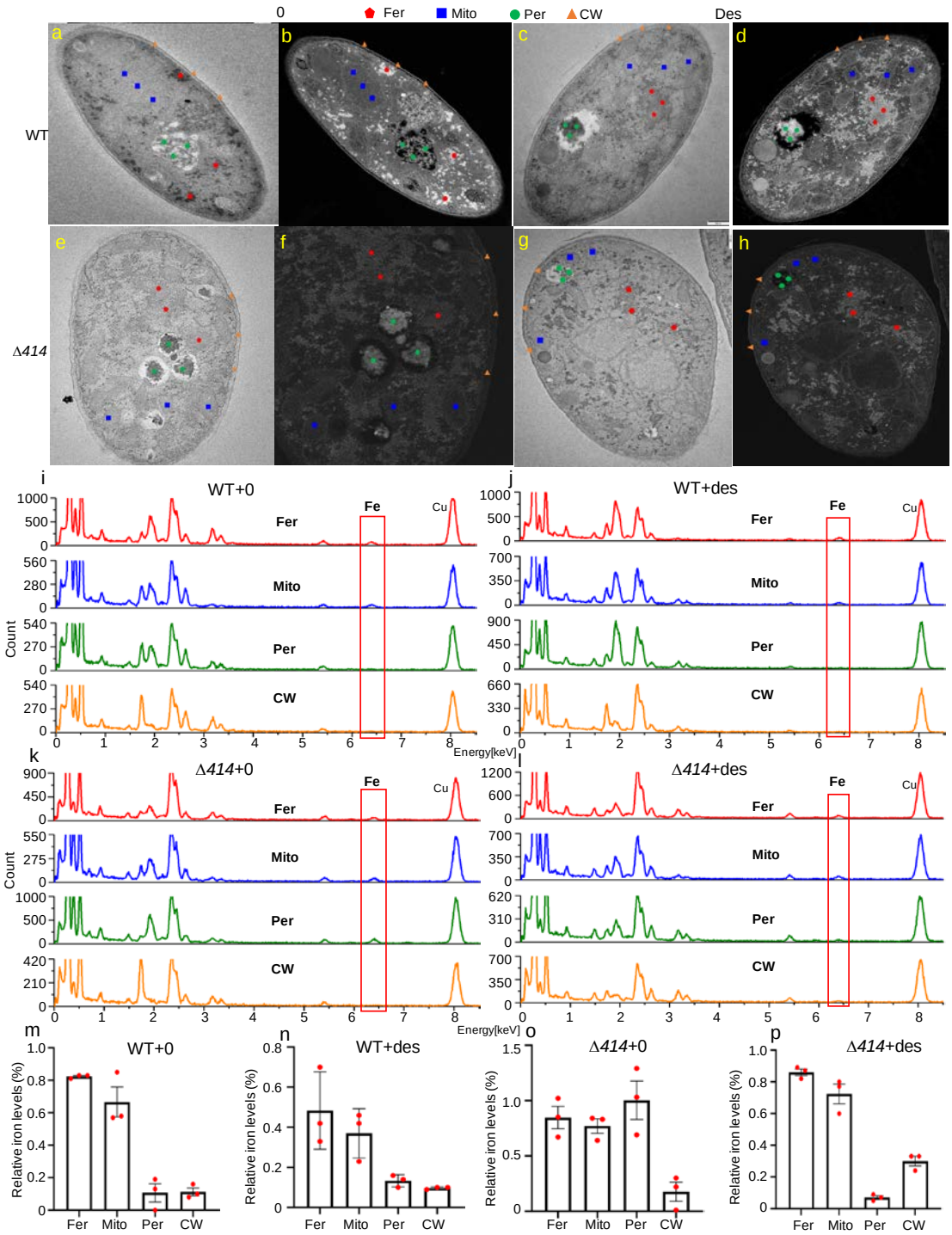

Fig. 2| Evaluation of the functions of desferriferrichrome in iron distribution and storage in *A. oligospora* mycelia. Δ*414*: Δ*Ao414*. Des: desferriferrichrome solution. 0: solvent as control. **a–h**, TEM image (**a, c, e, g**) and TEM-EDX electronic micrograph (**b, d, f, h**) of mycelia of WT and mutant Δ*Ao414* treated with and without desferriferrichrome, with analysis sites marked by different color indicators. Δ*414*: Δ*Ao414*. Fer: ferrichrome. Per: peroxisomes. Mito: mitochondria. CW: cell walls. **i–l**, X-ray spectra of different organelles within the same mycelial cell of WT and mutant Δ*Ao414*, treated with and without desferriferrichrome. **m–p**, Comparison of relative iron levels in different organelles within the same mycelial cell of WT and mutant Δ*Ao414*, treated with and without desferriferrichrome.

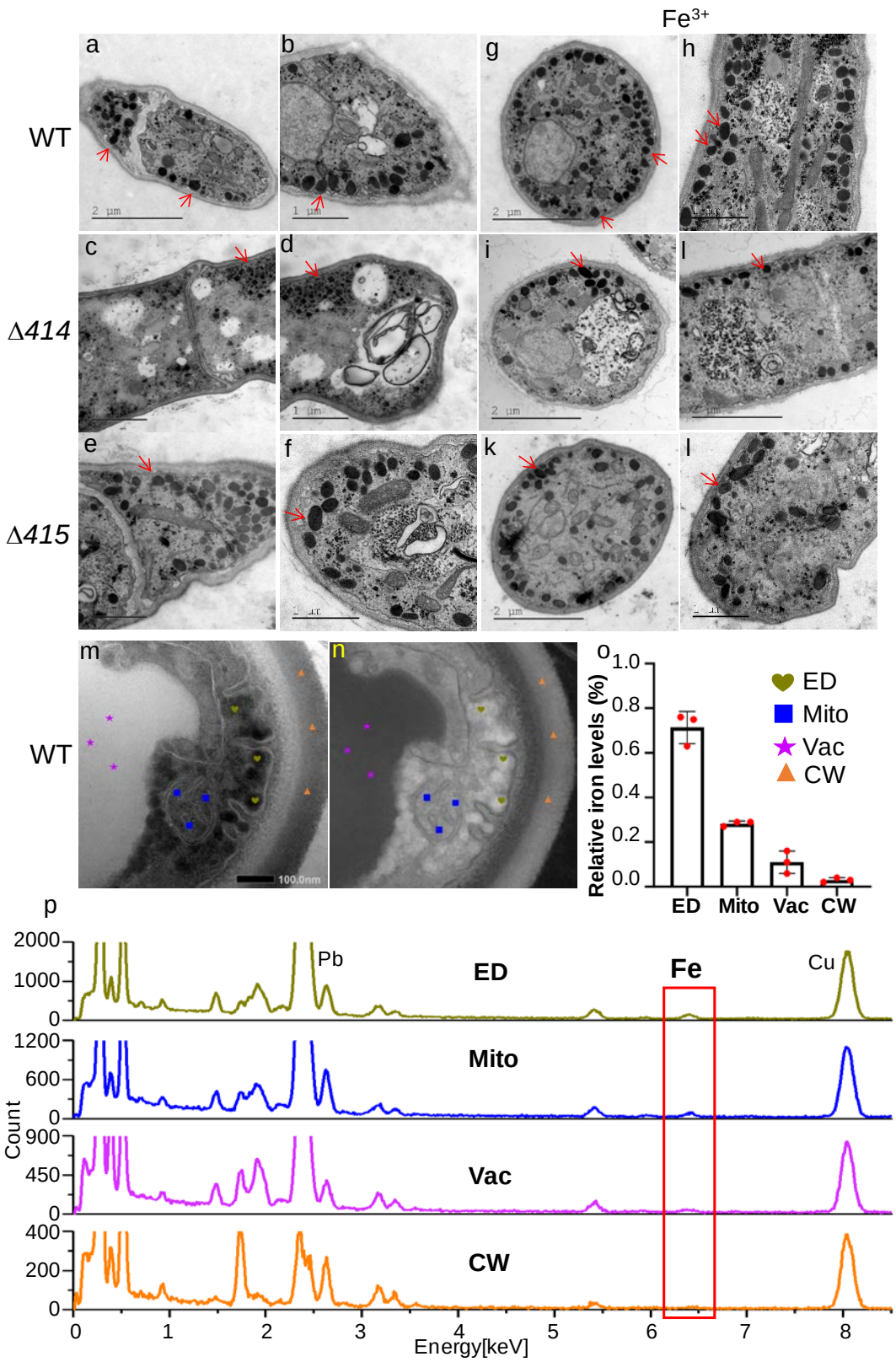

Fig. 3| Evaluation of desferriferrichrome functions in the organelles and iron distribution in the trapping devices of *A. oligospora*. a–f, TEM analysis of the organelles in trapping devices from WT (**a, b**), Δ*Ao414* (**c, d**) and Δ*Ao415* (**e, f**). Δ*414*: Δ*Ao414*. Δ*415*: Δ*Ao415*. Red arrow: electron dense body. **g–l**, TEM analysis of the organelles in trapping devices from WT (**g, h**), Δ*Ao414* (**i, j**) and Δ*Ao415* (**a, b**)

treated with 30μM ferric solution. Δ*414*: Δ*Ao414*. Δ*415*: Δ*Ao415*. Red arrow: electron dense body. **m**, **n**, TEM image (**m**) and TEM-EDX electronic micrograph (**n**) of WT trapping devices, with analysis sites marked by different color indicators. ED: electron dense body. Mito: mitochondria. Vac: Vacuole. CW: cell walls. **o**, X-ray spectra of different organelles within the same cell of WT trapping device. **p**, Comparison of relative iron levels in various organelles within the same cell of WT trapping devices.

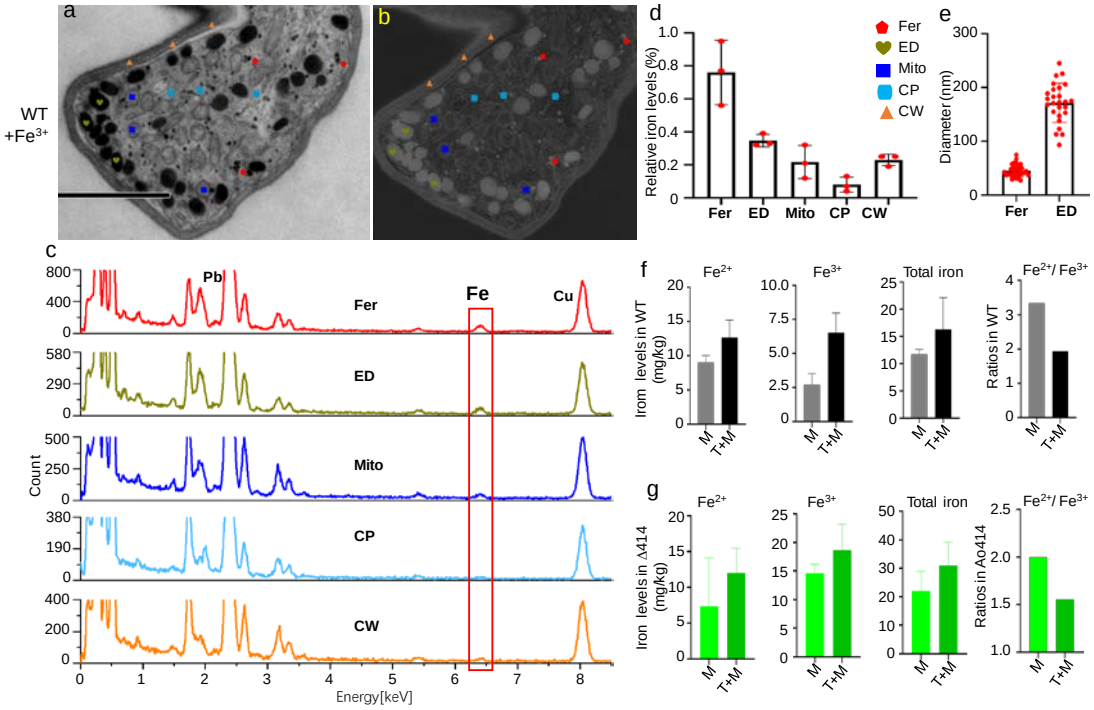

Fig. 4| Comparison of iron storages between ferrichrome organelles and electron dense bodies in *A. oligospora* WT treated with ferric. a, b, TEM image (**a**) and TEM-EDX electronic micrograph (**b**) of WT trapping device, with analysis sites marked by different color indicators. Fer: Ferrichrome. ED: electron dense body. Mito: mitochondria. CP: cytoplasm. CW: cell walls. **c,** X-ray spectra of different organelles within the same cell of WT trapping device. **d,** Comparison of relative iron levels in various organelles within the same cell of WT trapping device. **e,** Comparison of sizes between ferrichrome organelles and electron dense bodies in *A. oligospora*. **f,** Comparison of ferrous, ferric and total iron levels, as well as the ratios of ferrous to ferric iron between mycelia (M) and trapping devices (T) in WT. **g,** Comparison of ferrous, ferric and total iron levels, as well as the ratios of ferrous to ferric iron between mycelia (M) and trapping devices (T) in the mutant Δ*Ao414*.

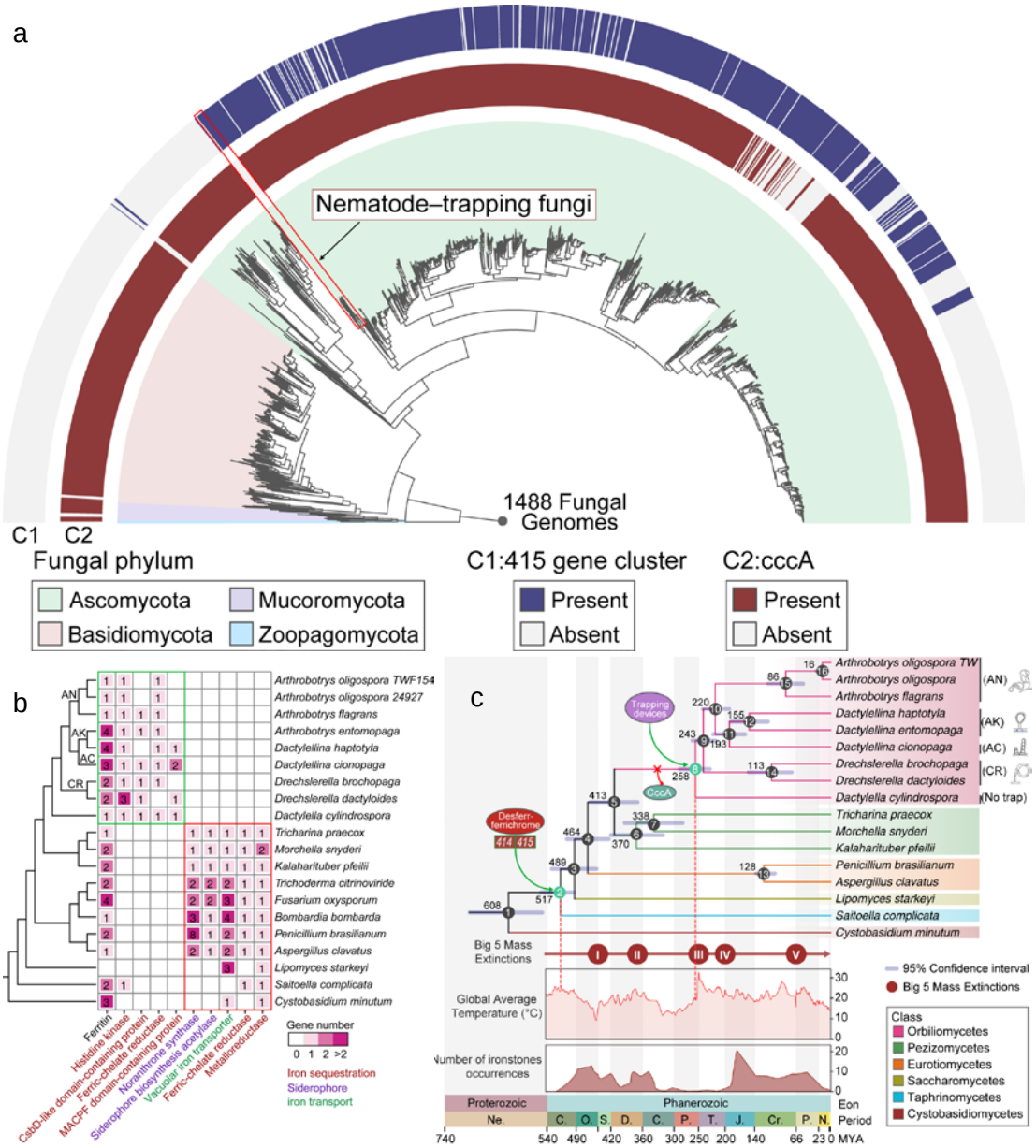

Fig. 5| Phylogeny and time-scale evolution analysis of fungal group with trapping devices in Ascomycota. a, Distribution patterns of the *Ao415* gene and the vacuole transport gene *cccA* in fungi kingdom. This panel highlights the presence and absence of these genes in fungal genomes. **b**, Heatmap illustrating the gain and loss of genes involved in iron sequestration and transport in NTFs, including ferritin, histidine kinase, CsbD-like domain-containing protein, ferric-chelate reductase, MACPF domain-containing protein, noranthrone synthase, siderophore biosynthesis acetylase, vacuolar iron transporter, ferric-chelate reductase and metalloreductase. The copy numbers of each gene are indicated in each color block. The tree topological structure is derived from the tree shown in panel A. **c**, Estimated divergence times of major lineages in the carnivorous Orbiliomycetes, with inferred occurrences of Phanerozoic ironstones and Phanerozoic global average temperature (GAT) trends. The chronogram was constructed using MCMCTree in the PAML package with 275,133 four-fold degenerate sites from 1136 single copy orthologous genes. Calibration was

based on three major events[42]: Ascomycota crown group (487–773 Mya), Orbiliomycetes–other Pezizomycotina (353–554 Mya), Saccharomycotina crown group (276–514 Mya) and one fossil calibration point (node 9: >100 Mya)[37]. Error bars represent the 95% highest posterior density (HPD) of node ages. Numbered circles at each node indicate node sequence from root to leaves, and node ages are shown. Circles labeled with Roman numerals represent major Phanerozoic mass extinction events: Late Devonian (375 Mya), Permian-Triassic (251.4 Mya), Triassic-Jurassic (201.4 Mya), and Cretaceous-Paleogene (66 Mya). Time periods are abbreviated as follows: De: Devonian, Ca: Carboniferous, Pe: Permian, Tr: Triassic, Ju: Jurassic, Cr: Cretaceous, P: Paleogene, N: Neogene.

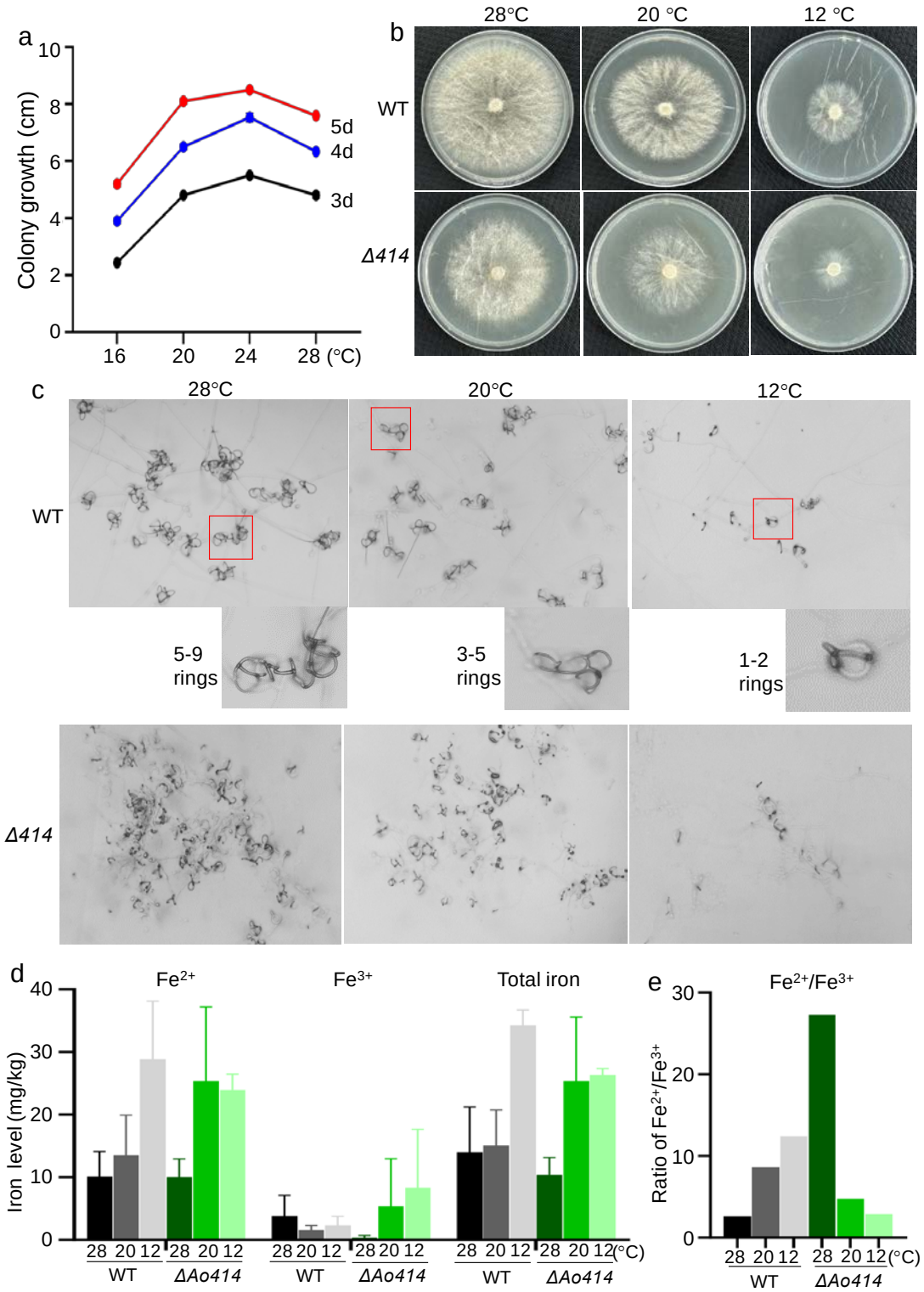

Fig. 6| Evaluation of the role of temperatures on colony growth, trapping devices, iron levels, and iron ratios in *A. oligospora*. a, The effect of temperature on colony growths in *A. oligospora* WT. **b,** Comparison of colony growths in WT and the mutant Δ*Ao414* at temperatures of 28°C, 20°C, and 12°C. **c,** Comparison of trapping devices in WT and the mutant Δ*Ao414* at temperatures of 28°C, 20°C, and 12°C. **d,** The effect of temperature on iron levels in fungal mycelia of WT and the mutant Δ*Ao414*. **e,** The effect of temperature on iron ratios in fungal mycelia of WT and the mutant Δ*Ao414*.

Material and Methods

Fungal strains and cultivation

YMF1.01883 (ATCC 24927) was procured from the State Key Laboratory for Conservation and Utilization of Bio-Resources and was cultivated at 25 °C for 3 to 4 days on a 9 cm Petri dish containing PDA (potato 200 g/L, glucose 10 g/L, agar 15 g/L, ddH_2O or tap water). Subsequently, 9 mm discs of the fungal colonies were transferred to 9 cm Petri dishes containing YMA (2 g/L yeast extract, 10 g/L maltose, agar 20 g/L) and incubated at 25 °C for 6 to 7 days. The spores were then washed with 20 mL of 0.05% Tween-80 mixed with approximately 3 mm glass beads.

Generation of gene deletion mutants

A modified homologous recombination method was employed to construct the mutants Δ*Ao414* and Δ*Ao415*. The upstream and downstream homologous arms of the target gene were cloned from A. oligospora YMF1.01883, and the *HygR* resistance sequence was cloned from a PUC19-1300-D-HYB vector using the Prime STAR Max enzyme (TsingKe, Beijing, China). All primers used in this study are listed in Table S1. The DNA fragments (5′ flank, hygromycin B, and 3′ flank) were purified using the RiboEXTRACT Universal DNA Purification Kit (Tsingke, China). The purified 5′ flank DNA fragment was inserted into the enzyme-digested PUC19-1300-D-HYB vector using the In-Fusion method to produce a PUC19-1300-D-HYB-5′ vector. Subsequently, the 3′ flank DNA fragment was inserted into this vector to generate a PUC19-1300-D-HYB-5′-3′ vector. The homologous fragment was amplified and purified as previously described. *A. oligospora* protoplasts were prepared as previously described. The purified homologous fragment was transformed into *A. oligospora* protoplasts. Transformation colonies were selected after incubation at 28 °C for 2−4 days, and each colony was transferred to a new plate containing PDA. After incubation at 28 °C for 5 days, genomic DNA of putative transformants was extracted and verified by polymerase chain reaction (PCR) to check for the integration of the target gene into the genome. Mutants deficient in the target gene were screened by PCR and confirmed by sequencing analysis. Further confirmation of the mutants was performed by Southern blot hybridization using the North2South Chemiluminescent Hybridization and Detection Kit according to the manufacturer's instructions (Pierce, Rockford, IL). For Southern blot analysis, restriction enzyme HindIII was used to digest WT and Δ*Ao414* genomic DNA, and restriction enzyme SmaI was used to digest WT and Δ*Ao415* genomic DNA (Extended Data Fig. S1).

Development of trapping device

To facilitate the collection of mycelia, *A. oligospora* YMF1.3170 was cultured at 25 °C for 3 to 4 days on 9 cm Petri dishes containing potato dextrose agar (PDA) with cellophane (4 cm diameter, area 50.24 cm^2). *Caenorhabditis elegans* N2 was grown in a 250 mL flask with oatmeal agar medium (oatmeal 30 g, water 20 mL) for 7 days. The nematodes were then collected from the flask's walls and transferred to a 2 mL microcentrifuge tube[57]. To prepare the nematode suspension, 1 mL of double-distilled water was added and mixed. The nematode concentration was subsequently adjusted to 300 nematodes per 200 µL for the assay. The wild-type (WT) and mutant strains were exposed to 200 µL of double-distilled water containing 300 nematodes to induce the formation of trapping devices, classified as the mycelia + trapping devices (M+T) group. The control group, which only included mycelia (M), was treated with 200 µL of double-distilled water without nematodes.

Desferriferrichrome assay

Five milligrams of desferriferrichrome (CAS No. 34787-28-5, Sigma Co.) were dissolved in 5 mL of dimethyl sulfoxide (DMSO) to prepare a 1 mg/mL desferriferrichrome stock solution. To achieve a final concentration of 1.45 μM desferriferrichrome, 150 μL of the 1 mg/mL stock solution was added to 150 mL of potato dextrose broth (PDB). Wild-type (WT) and mutant strains, cultured on potato dextrose agar (PDA) for 7 days, were inoculated into potato dextrose (PD) broth (200 g/L potatoes, 20 g/L glucose) and incubated on a shaker at 180 rpm for 12 hours. The culture was then supplemented with 1.45 μM desferriferrichrome and further incubated on the shaker for another 12 hours. The mycelia were harvested, fixed with 2.5% glutaraldehyde, and examined using transmission electron microscopy (TEM).

Fe^{3+}Assay

The fungal strains were initiated with 9 cm diameter hyphal disks at 28°C for 6 days on the plates of PDA supplemented with or without $FeCl_3 \cdot 6H_2O$ (10–30 μM) and then about 400 nematodes were introduced to the cultures. After 12 h, traps and captured nematodes per plate were observed under a microscope and counted at specific time-points. The diameter of each colony was measured and then calculated with GraphPad 9.3.4.

Iron contents

An iron assay kit (#ab83366, Abcam) was used to evaluate intracellular iron levels (Fe^{2+} and Fe^{3+}) in fungi[49]. First, mycelia (20–80 mg) were collected in phosphate-buffered saline (PBS) containing 80 g NaCl, 2 g KCl, 14.4 g Na_2HPO_4, and 2.4 g KH_2PO_4 in 1 L of double-distilled water. The mycelia were then homogenized in iron assay buffer using a Dounce homogenizer on ice with 50–100 passes. Next, iron reducer was added to the collected supernatant, mixed, and incubated. Following this, iron probe (3-(2-Pyridyl)-5,6-bis(5-sulfo-2-furyl)-1,2,4-triazine, disodium salt) was added, mixed, and incubated for 1 hour. The resulting solution was immediately measured using a microplate reader at OD = 593 nm. To account for the effects of nematodes on iron content in the mycelia + trapping devices (M+T) groups, nematodes were removed from the M+T samples using a 10 μL pipette. Additionally, the iron content of 300 nematodes was measured separately. Iron content in the M+T groups, both with and without nematodes, was evaluated using the same method. All mycelia were collected, weighed, and suspended in double-distilled water at a 1:10 ratio. The suspension was ground using an ultrasonic cell disruptor to obtain a uniform mixture, from which 1 mL was taken for analysis. Similarly, 300 nematodes were suspended in 1 mL of distilled water, ground using an ultrasonic cell disruptor, and then centrifuged at 16,000 rpm for 10 minutes to separate the supernatant for further experiments.

Transmission electron microscopy (TEM)

For transmission electron microscopy (TEM) analysis, ultrathin sections of hyphal cells were prepared and examined as previously described[49]. The samples were pretreated with 4% paraformaldehyde and then incubated overnight at 4 °C with 2.5% glutaraldehyde (Sigma) in phosphate buffer (pH 7.4). Following this, the samples

were post-fixed in 1% osmium tetroxide (OsO_4). They were then dehydrated through a gradient ethanol series, embedded in Spurr resin, and stained with 2% uranyl acetate and Reynold's lead citrate. Finally, the samples were examined using an H-7650 transmission electron microscope (Hitachi, Tokyo, Japan).

Transmission electron microscopy-energy dispersive X-ray spectroscopy (TEM-EDX)

The distributions of elements within the samples were qualitatively determined according to the method conducted by Sheraz et al.[58]. In detail, the mycelia or trapping devices were placed in a primary fixative consisting of 2.5% (v/v) glutaraldehyde for approximately 6 hours at 4 °C. The samples were then washed three times at 15-minute intervals with phosphate-buffered saline (PBS) buffer (0.1 mol/L, pH 6.8), followed by post-fixation in 1% (m/v) osmium tetroxide for 2 hours at 4 °C. After washing with PBS buffer, the samples were dehydrated through a graded ethanol series: 30% (v/v) for 15 minutes, 50% (v/v) for 15 minutes, 70% (v/v) for 15 minutes, 80% (v/v) for 15 minutes, 90% (v/v) for 15 minutes, and 100% (v/v) for 15 minutes, twice. Prior to embedding, the samples were infiltrated with a mixture of anhydrous ethanol and epoxy resin EPON-812 (1:1, v/v) overnight. The samples were then placed in an oven at 60 °C for 48 hours and finally stored in desiccators.

Structures were further sectioned into ultrathin slices using an ultramicrotome (Leica RM2016, Germany). The resulting 100-nm ultrathin sections were mounted on 200-mesh copper TEM grids (Agar Scientific). Where indicated, sections were stained with 1% uranyl acetate for 15 minutes, followed by Reynold's lead citrate (Reynolds, 1963) for 7 minutes. Samples were then observed using a JEOL 1400 transmission electron microscope (JEOL, Akishima, Japan) at 80 kV. To qualitatively determine the distribution of elements within the samples, stained sections were analyzed to identify iron (Fe) deposits and quantify Fe content through X-ray microanalysis. Energy dispersive X-ray spectroscopy (EDAX, USA), equipped with the TEM, was employed for this purpose. Circular regions of interest were selected for energy-dispersive X-ray (EDX) analysis. An electron beam with an acceleration voltage of 200 kV and a spot size of 10 nm was focused on the specimen, and X-ray spectra were collected for approximately 100 seconds. X-rays were detected using an Oxford INCAx-sight detector (Oxford Instruments, Abingdon, UK) and analyzed with the Oxford INCA SUITE v.4.02. The Zeta factor method was used for standardless quantitative analysis, checking elements manually selected and reporting elements excluded from qualitative analysis.

Genome data collection and quality assessment

To investigate the distribution of a genomic element within the fungal kingdom, we downloaded all published genome and corresponding annotation files from the JGI Mycocosm database (15 December 2022). Additionally, we used "Orbiliomycetes" as a search term in NCBI's Genome Browser to retrieve all genome assemblies with gene annotation files for this class. In total, 2,175 fungal genomes were collected. For each predicted gene, the longest transcript was extracted as the representative transcript. Protein sequences for each genome were generated using gffread

(v.0.9.12)[59]. To assess the quality of the gene sets for use in phylogenomic analyses, we evaluated their completeness using Benchmarking Universal Single-Copy Orthologs (BUSCO) (v.3.0.2)[60] based on the fungi_odb10 lineage dataset (2021-06-28). Genes were categorized as "single copy" if only one complete predicted gene was present in the genome, "duplicated" if two or more complete predicted genes were found for one BUSCO gene, "fragmented" if the predicted gene was shorter than 95% of the aligned sequence lengths from 50 different fungal species, and "missing" if no predicted gene was present. Only genomes with a BUSCO completeness of 90% or higher were considered high-quality and retained. In total, 1,488 high-quality fungal genomes were retained (1,177 Ascomycota; 289 Basidiomycota; 21 Mucoromycota; 1 Zoopagomycota), representing 1,229 species: Ascomycota (n=996), Basidiomycota (n=233), Mucoromycota (n=19), and Zoopagomycota (n=1) (Table S2).

Screening of iron sequestration, transports, and siderophore related genes

Genes classified as having ferric-chelate reductase activity (GO:0000293) were considered to be involved in iron sequestration. Genes associated with iron ion transmembrane transport (GO:0034755) were identified as involved in iron transport. Genes categorized under siderophore biosynthetic process (GO:0019290), siderophore metabolic process (GO:0009237), and siderophore transport (GO:0015891) were deemed to be involved in siderophore-related processes. Additionally, ferritin, a common iron storage protein, was also included.

Identification homologue of *Ao415* biosynthetic gene cluster in the fungal kingdom

The biosynthetic gene clusters for each genome were annotated using antiSMASH 7.0 (v.7.0.0)[61] via the command-line version with default parameters, except for the argument '--taxon fungi'. In total, 67,350 secondary metabolism gene clusters were annotated from 1,488 fungal genomes. A local database was created from GenBank sequences of all gene clusters using the 'cblaster makedb' module (v.1.3.18)[62]. To identify gene clusters homologous to the Ao415 gene cluster within the fungal kingdom, the search function of cblaster was employed to query the amino acid sequences of the seven genes in the Ao415 gene cluster (Ao410–Ao416) against the local database. Both Ao414 and Ao415 needed to be represented in a hit cluster, and the minimum percent identity for a BLAST hit was set to 30%. We identified 744 fungal genomes containing Ao415 gene cluster homologues, all of which were from Ascomycetes. The presence and absence of the Ao415 gene cluster were mapped onto a phylogenetic tree (containing 1,488 high-quality fungal genomes) extracted from the MycoCosm portal to visualize the distribution of the Ao415 gene cluster within the fungal kingdom.

Inference of homologous groups

To better understand the evolutionary trajectory of the Ao415 biosynthetic gene cluster within the fungal kingdom, we selected 17 representative fungi (9 Orbiliomycetes, 3 Pezizomycetes, 2 Eurotiomycetes, 1 Saccharomycetes, and 1 Taphrinomycetes) containing the Ao415 gene cluster, as well as 1 fungus from Cystobasidiomycetes lacking the Ao415 gene cluster, to serve as an outgroup. This selection was guided by the fungal species tree from the MycoCosm portal. Protein sequences from these 17 fungal genomes, totaling 131,694 sequences, were subjected to all-versus-all BLASTP (v.2.11.0+). The resulting output was then analyzed using

OrthoFinder (v.2.5.2)[63] for gene family clustering, employing the MCL algorithm with an inflation factor set to 1.5. This analysis identified 1,136 sets of 1:1 orthologous protein-coding genes.

Function annotations of homologous groups

To assign function annotations to each homologous group (OG), we selected a representative sequence for each group. First, we ordered the sequences within each OG by their lengths using the 'sortbylength' option in USEARCH11 (v.11.0.667)[64]. Next, we employed the UCLUST algorithm to cluster the sequences within each OG based on 30% amino acid sequence similarity. The sequence with the highest abundance in each OG was designated as the representative sequence. In cases of equal abundance, the longest sequence was chosen as the representative. For each representative sequence, gene function and gene ontology (GO) were predicted using the PANNZER2 web server[65].

Phylogenetic analyses and divergence times estimating

Amino acid sequences for each orthogroup were aligned using MAFFT (v.7.505) with the 'auto' parameter. Codon alignments were generated from these MAFFT-aligned amino acid sequences using PAL2NAL (v14) with default parameters. The aligned amino acid sequences and their corresponding codon alignments were concatenated to construct amino acid (AA) and nucleotide (NT) data matrices, respectively. For the AA data matrix, the best substitution model was determined using the "-m TEST" parameter, which estimates the optimal model based on Bayesian Information Criterion (BIC) values. Maximum likelihood (ML) trees with 1,000 bootstrap iterations were constructed according to the best-fitting model using IQ-TREE2[66]. Fourfold degenerate sites were extracted from the NT data matrix using the open-source tool get4foldSites (https://github.com/brunonevado/get4foldSites). Divergence times for all nodes were estimated with MCMCTree from the PAML package, using 275,133 fourfold degenerate sites from 1,136 single-copy orthologous genes. Calibration was based on three major events[42]: Ascomycota crown group (487–773 Mya), Orbiliomycetes–other Pezizomycotina (353–554 Mya), Saccharomycotina crown group (276–514 Mya) and one fossil calibration point (node 9: >100 Mya)[37]. The clock model was set to independent rates, with a burn-in of 20,000, 100,000 samples, a sampling frequency of 10, and the JC69 model. Tracer v.1.7.1[67] was used to visually check the convergence of parameters across replicate MCMC chains. All resulting effective sample sizes (ESS) ranged from 275 to 1,299 (Table S3), indicating that the parameters across replicate MCMC chains achieved convergence (with ESS values expected to exceed 200).

RNA-seq data analysis

Raw reads from both WT and ΔAO414 samples were examined using FastQC. To obtain clean data, fastp (v.4.10.0)[68] was used with default parameters to filter adaptor sequences and remove low-quality reads. The reference genome and gene model annotation files for A. oligospora ATCC 24927 were downloaded from NCBI's Genome Browser. Genome indexing was performed using 'hisat2-build' in Hisat2 (v.2.2.1)[69], incorporating splice sites and exon information. The filtered paired-end reads were aligned to the reference genome using Hisat2. Gene abundance for each sample was estimated using featureCounts (v.2.0.3)[70] from the aligned BAM files. Differential expression analysis was conducted using the DESeq2 R package (v.1.30.1)[71]. DESeq2 employs statistical tests to identify differential expression in

digital gene expression data based on the negative binomial distribution. Resulting p-values were adjusted using the Benjamini–Hochberg approach to control the false discovery rate.

Temperature and metal ion assays

Conidial suspensions (50 μL) were collected and quantified using a hemocytometer. Subsequently, 100 μL of fungal spore suspensions (800 spores/μL) were added to 6 cm Petri dishes containing water agar (20 g/L agar in 1 L double-distilled water (ddH_2O). Water agar prepared with tap water (Kunming Water Supply Company) was used as a negative control. All fungal dishes were incubated at 12 °C, 20 °C, and 28 °C for 7 days. Trapping devices on each plate were observed and counted under a microscope. For colony growth analysis, fungal strains were cultivated on 9 cm diameter PDA plates at 16 °C, 20 °C, 24 °C, and 28 °C for 6 days, and the diameter of each colony was measured. All experiments were conducted with at least three replicates.